Organic & Biomolecular Chemistry

PAPER

CrossMark
click for updates

Understanding the conformational behaviour of Ac-Ala-NHMe in different media. A joint NMR and DFT study†

Rodrigo A. Cormanich,[a] Michael Bühl[b] and Roberto Rittner*[a]

The conformational behaviour of Ac-Ala-NHMe was studied in the gas-phase and in solution by theoretical calculations (B3LYP-D3/aug-cc-pVDZ level) and experimental ^{1}H NMR. The conformational preferences of this compound were shown to result from a complex interplay between the strengths of possible intramolecular hydrogen bonds, steric interactions, hyperconjugation, entropy effects and the overall dipole moments. The Ac-Ala-N(Me)$_2$ derivative was studied in addition, to design a system akin to Ac-Ala-NHMe, but with disrupted intramolecular hydrogen bonds involving the -NHMe group, mimicking the effect of polar protic solvents.

Introduction

The conformational behaviour of individual building blocks for amino-acid residues has been widely studied in the literature in order to find the lowest energy conformers and, possibly, to understand the folding pathways of biological macromolecules built from these compounds.[1] Alanine, as the simplest chiral amino acid, is being widely studied both experimentally and theoretically.[2] In order to model individual amino acids in a peptide environment, compounds of the general formula Ac-R-NHMe (R = amino acid) are being studied.[3] In particular, Ac-Ala-NHMe is the most studied compound among the natural amino acid residues.[4] Papers studying Ac-R-NHMe compounds that may be found in the literature are increasing based on theoretical and gas phase experimental techniques to complement work dealing with these models in solution.

As part of a wider research programme, we have studied amino acids,[5] amino acid methyl esters[6] and peptide model derivatives[7] in many different solvents. Recently, we have used vibrational and NMR spectroscopy in conjunction with detailed DFT calculations to elucidate and rationalise the conformational behaviour of Ac-Gly-NHMe in solution.[7] Commonly such conformational preferences are mainly interpreted in terms of intramolecular hydrogen bonds (IHBs). However,
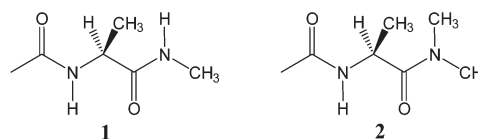
Scheme 1 Ac-Ala-NHMe (**1**) and Ac-Ala-N(Me)$_2$ (**2**) structure representations.

other effects such as steric hindrance and hyperconjugation, are well known to be ubiquitous and to influence the geometry/energy of systems much simpler than dipeptide models.[8] In fact we have shown that the conformational preferences of Ac-Gly-NHMe, which change considerably from nonpolar to polar solvents, are strongly influenced by hyperconjugation and steric interactions.[7] We have now extended these studies to the Ac-Ala-NHMe dipeptide model (**1**, Scheme 1), employing experimental ^{1}H NMR spectroscopy and theoretical calculations. As previously done for Ac-Gly-NHMe, we also included the Ac-Ala-N(Me)$_2$ derivative (**2**), in order to study the effect of IHB on the Ac-Ala-NHMe conformational isomerism.

Experimental

NMR spectra

Compounds **1** and **2** were purchased from Ukrorgsyntez Ltd. (UORSY) and used without further purification. ^{1}H NMR experiments were recorded on a Bruker Avance-III spectrometer operating at 600.17 MHz for [1]H. Spectra were recorded in solutions of *ca.* 1 mg in 0.7 mL of CD$_2$Cl$_2$, acetone-d$_6$, acetonitrile-d$_3$, DMSO-d$_6$, CD$_3$OH and H$_2$O (18.2 MΩ cm from a

[a]Chemistry Institute, University of Campinas, Campinas, SP 13083-970, Brazil.
E-mail: rittner@iqm.unicamp.br; Fax: +(19) 3521 3023; Tel: +(19) 3521 3150
[b]EastChem School of Chemistry, University of St Andrews, North Haugh, St Andrews, Fife KY16 9ST, UK. Fax: +01334 463800; Tel: +01334 467171

Millipore system). An insertion tube with D_2O in the H_2O sample was used in order to maintain the field-frequency lock and avoid deuteration of the N–H bonds. Commercial solvents were referenced to internal TMS. Typical conditions used were as follows: a probe temperature of 25 °C, from 8 to 128 transients (depending on solute solubility), a spectral width of ~6.0 kHz, 64 k data points, an acquisition time of ~5.5 s and zero-filled to 128 k points. Also, homonuclear decoupling was performed through the nuclear magnetic double resonance experiment[9] in order to measure spin–spin coupling constants (SSCCs) from N(H)–C(H)–CH_3 Ac-Ala-NHMe and Ac-Ala-N(Me)$_2$ spin systems. ^{1}H NMR spectra are provided in the ESI.†

Computational details

Conformers of compounds **1** and **2** were located through a Monte Carlo conformational search at the B3LYP/6-311+G* level with the Spartan 14 program,[10] using a 10 kcal mol^{-1} threshold and 5000 K initial temperature in the simulated-annealing algorithm. Optimisations and frequency calculations were carried out at the B3LYP-D3/aug-cc-pVDZ level using the Gaussian 09 program, Revision D.01[11] for all conformers found in the Monte Carlo calculations. This theoretical level showed good performance for the Ac-Gly-NHMe in comparison to CCSD(T)/aug-cc-pVTZ level in our previous work.[7] The lack of negative harmonic vibrational frequencies confirmed that all conformers are true energy minima. The same frequency calculations were used to evaluate thermodynamic corrections affording enthalpies and Gibbs free energies at ambient, standard temperature and pressure for each conformer. Solvent effects were evaluated by optimising each conformer using an implicit solvent model, namely the IEF-PCM (integral equation formalism variant of the Polarizable Continuum Model)[12] at the B3LYP-D3/aug-cc-pVDZ level.

Using B3LYP-D3/aug-cc-pVDZ optimised structures for the isolated compounds (gas phase), spin–spin coupling constants (SSCCs) were computed with Gaussian09 at the BHandH/EPR-III theoretical level.[13,14] Employing a basis set that was optimised for the computation of the Fermi-contact component of SSCCs,[15] this level has shown a very good performance in the computation of a very large variety of spin–spin

coupling constants (SSCCs) involving carbon, fluorine and hydrogen atoms.[16] Fully optimised geometries obtained from B3LYP-D3/aug-cc-pVDZ calculations were used to run NBO (Natural Bond Orbitals)[17] calculations on the same level for the isolated compounds. Also, electron densities obtained from B3LYP-D3/aug-cc-pVDZ for the optimised conformers were used to run QTAIM (quantum theory of atoms in molecules),[18] ELF (electron localization functions),[19] NCI (non covalent interactions)[20] and DORI (density overlap regions indicator)[21] calculations on AIMALL,[22] TopMod[23] and NCIPLOT 3.0[20] programs.

Results and discussion

The experimental ^{1}H chemical shifts and $^3J_{HH}$ spin–spin coupling constants of compounds Ac-Ala-NHMe (**1**) and Ac-Ala-N(Me)$_2$ (**2**) are collected in Tables 1 and 2, respectively. Both compounds show only relatively minor changes of their $^3J_{HaHb}$ values in different solvents. Based on the well known Karplus relationship,[24] such result could suggest that the conformer populations of these two compounds are not very sensitive to solvent effects.

The Monte Carlo conformational searches for compounds **1** and **2** afforded 12 conformers each. For the relative potential (ΔE) enthalpic (ΔH) and entropic (ΔG) energy values and graphical representations see Tables S1–S6 and Fig. S1 and S2 in the ESI.† Fig. 1 shows the geometric representations obtained at the B3LYP-D3/aug-cc-pVDZ level for the most stable conformers of compounds **1** and **2**. The calculated populations for these most stable conformers, obtained from ΔG energies (B3LYP-D3/aug-cc-pVDZ level) in different media (IEF-PCM), are shown in Table 3. These results show that conformer populations change only slightly with the solvent dielectric constant. Conformers with higher calculated dipole moments (μ) have slightly increased populations in solvents of higher dielectric constant and *vice versa*.

The SSCC values were obtained by theoretical calculations for all conformers of a given compound through averaging

Table 1 Experimental chemical shift (ppm) and $^3J_{HH}$ spin–spin coupling constant (Hz) values for the Ac-Ala-NHMe in solvents of different dielectric constants (ε)

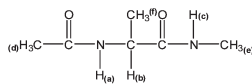| Solvent	ε	$\delta H_{(a)}$	$\delta H_{(b)}$	$\delta H_{(c)}$	$\delta H_{(d)}$	$\delta H_{(e)}$	$\delta H_{(f)}$	$^3J_{HaHb}$	$^3J_{HbHf}$	$^3J_{HcHe}$
CD_2Cl_2	9.8	6.44	4.41	6.49	1.95	2.75	1.32	7.56	6.96	4.80
Acetone-d_6	20.7	7.21	4.35	7.27	1.90	2.68	1.25	7.62	7.08	4.74
CD_3CN	37.5	6.63	4.23	6.71	1.92	2.68	1.27	7.20	7.14	4.74
DMSO-d_6	46.7	7.77	4.19	8.00	1.82	2.56	1.15	7.68	7.14	4.62
CD_3OH	32.7	7.91	4.28	8.18	1.97	2.72	1.31	6.90	7.14	4.68
$H_2O : D_2O$	80.1	8.25	4.21	7.93	2.01	2.73	1.34	—	7.26	4.02

Table 2 Experimental chemical shift (ppm) and $^3J_{HH}$ spin–spin coupling constant (Hz) values for the Ac-Ala-NMe$_2$ in solvents of different dielectric constants (ε)

| Solvent	ε	$\delta H_{(a)}$	$\delta H_{(b)}$	$\delta H_{(c)/(d)}{}^a$	$\delta H_{(c)/(d)}{}^a$	$\delta H_{(e)}$	$\delta H_{(f)}$	$^3J_{HaHb}$	$^3J_{HbHf}$
CD$_2$Cl$_2$	9.8	6.56	4.83	3.04	2.92	1.93	1.28	7.32	6.78
Acetone-d$_6$	20.7	7.10	4.82	3.08	2.88	1.89	1.19	7.80	6.84
CD$_3$CN	37.5	7.38	5.33	3.58	3.42	2.42	1.76	7.56	6.90
DMSO-d$_6$	46.7	8.06	4.69	3.00	2.81	1.81	1.13	7.86	6.90
CD$_3$OH	32.7	8.18	4.80	3.12	2.94	1.95	1.27	6.96	6.96
H$_2$O : D$_2$O	80.1	—	—	3.13	2.96	2.00	1.29	—	7.14

^{a} H$_{(c)}$ and H$_{(d)}$ were not assigned; according to the calculated mean shieldings of the Me protons in the isolated molecules, it is the Me group in *trans* position to the CO group that has the higher shielding (*i.e.* smaller chemical shift).

over all conformers according to the following Boltzmann distribution:

$$J_{\text{calc}} = \sum_{i=1}^{n} \frac{\eta_i}{\eta_T} J_i \qquad (1)$$

where

$$\frac{\eta_i}{\eta_T} = \frac{e^{-\Delta G_i/RT}}{\sum_{i=1}^{n} e^{-\Delta G_i/RT}} \qquad (2)$$
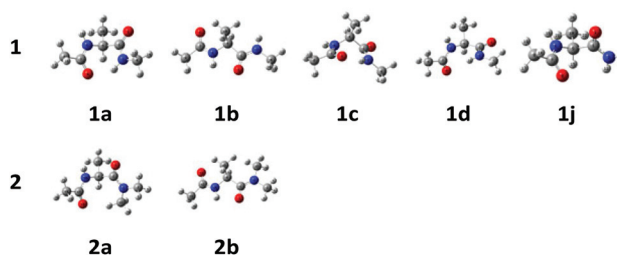
Fig. 1 B3LYP-D3/aug-cc-pVDZ optimised geometries of the most stable conformers of compounds **1** and **2**.

ΔG_i is the relative energy of conformer "*i*" and T is the temperature in Kelvin, which in this case is the room temperature (298.15 K).

Plotting the corresponding averaged $^3J_{HaHb}$ theoretical SSCCs obtained for compound **1** in different media in comparison to experimental values (Fig. 2a), one may observe that the calculated SSCCs are underestimated in terms of absolute values, but the experimental trend, *i.e.*, slow variation of SSCCs upon changing the medium, is well reproduced by the theoretical calculations. The same result is observed for compound **2** (Fig. 2b).

According to these calculations, compound **1** has 5 conformers with considerable population values (**1a–1d** and **1j**), while compound **2** has only **2a** and **2b** (Fig. 1 and Table 3). In compound **1**, conformer **1a** is the most stable for the isolated compound, but its population decreases considerably with the increase of dielectric constant of the surrounding medium, due to the relative low calculated dipole moment (Table 3). On the other hand, conformer **1d**, which has the highest dipole moment and a negligible population value for the isolated compound, becomes approximately isoenergetic to conformer **1b** in water. Conformer **1b** is the most stable in all solvents. It is interesting to note that the calculated dipole moment of

Table 3 Conformer populations (in %) of compounds **1** and **2** from Gibbs free energies (ΔG) obtained at the B3LYP-D3/aug-cc-pVDZ level for the isolated compound and in different IEF-PCM solvents

	1a		1b		1c		1d		1j		2a		2b	
	%P	μ	%P	μ	%P	μ	%P	μ	%P	μ	%P	μ	%P	μ
Isolated	64.7	2.80	30.7	3.12	1.5	3.67	2.8	5.02	—^{a}	—^{a}	22.3	0.56	77.3	3.35
CH$_2$Cl$_2$	24.2	3.79	54.7	3.95	0.6	4.75	18.7	8.16	7.4	4.80	25.1	2.14	74.4	4.45
Acetone	17.0	3.92	41.0	4.06	0.5	4.89	20.8	8.62	18.7	4.83	23.2	3.26	75.7	4.28
CH$_3$CN	19.8	3.97	46.2	4.10	0.6	4.95	30.7	8.78	12.6	5.09	25.4	4.84	73.2	4.63
DMSO	17.1	3.99	39.0	4.11	0.5	4.96	28.8	8.83	12.0	5.11	25.8	4.90	72.7	4.64
CH$_3$OH	17.3	3.97	40.7	4.09	0.5	4.94	26.1	8.76	13.0	5.03	25.0	4.82	73.7	4.62
H$_2$O	16.4	4.00	36.8	4.13	0.5	4.98	32.0	8.91	11.6	5.20	25.7	4.97	72.6	4.66

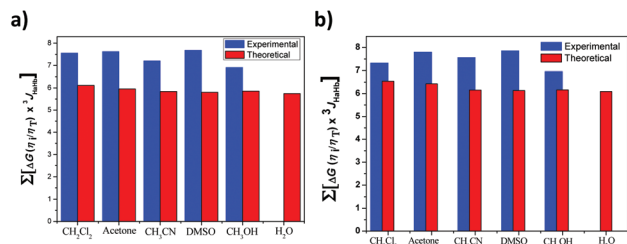^{a} Conformer **1j** is interconverted to the more stable conformer **1a** for the isolated compound.

Fig. 2 Comparison between experimental and theoretical obtained $^3J_{HaHb}$ SSCCs for compounds **1** (left) and **2** (right). Theoretical values were obtained by averaging all conformer contributions for the $^3J_{HaHb}$ values.

$n_{O(1)} \to \sigma^*_{N-H}$ $n_{O(1)} \to \sigma^*_{N-H}$ $n_{O(1)} \to \sigma^*_{N-H}$ $n_N \to \sigma^*_{N-H}$

$n_{O(1)} \to \sigma^*_{N-H}$ $n_{O(2)} \to \sigma^*_{N-H}$ $n_{O(2)} \to \sigma^*_{N-H}$

Fig. 3 QTAIM, ELF, NCI, DORI and NBO graphical representations for conformers **1a–1d** and **1j**. QTAIM green points and red points represent bond critical points and ring critical points, respectively. NCI figures were obtained with a blue–green–red scale ranging from $-0.02 <$ sign $\lambda_2 < 0.02$ au and with a RDG cutoff of 0.5 au. ELF localization domains were built with a 0.8 au isodensity value. DORI were also obtained with a blue–green–red scale ranging from $-0.02 <$ sign $\lambda_2 < 0.02$ au. NBO plots of orbitals involved in $n \to \sigma^*_{NH}$ interactions were obtained with an isovalue of 0.04 au. All figures were obtained from B3LYP/aug-cc-pVDZ electron densities at B3LYP-D3/aug-cc-pVDZ optimised geometries.

conformer **1b** is just a little higher than conformer **1a**, but that their relative population is almost inverted on going from the isolated compound to CH_2Cl_2 solution. Thus, another effect rather than dipole moment stabilisation by solvation alone is operating to make conformer **1b** the most stable in higher polar media.

Conformer **1a** and **1c** should be stabilised by a strong 7-membered NH···O=C IHB resulting in a "folded" geometry, while conformer **1b** has an "extended" geometry and may form a weak 5-membered NH···O=C IHB, and **1d** has a high calculated dipole moment and may form a weak 5-membered NH···N IHB. The folded geometries have an entropic penalty in comparison to the extended geometries, which may be observed in the difference between the raw potential relative energies for the isolated conformers (Table S1 in the ESI†) and their relative Gibbs free energies (Table S3 in the ESI†). The entropic penalty alone cannot explain why conformer **1a** becomes less stable than **1b** in CH_2Cl_2, since conformer **1a** is more stable than **1b** when this effect is taken into account for the isolated compound (Table 3). Thus, the interplay between entropy and dipole moments may explain the conformational population changes of compound **1** in different media.

In order to evaluate IHB formation and its influence on conformational energies and geometries for the isolated conformers, we applied the QTAIM, NCI, ELF and DORI topological approaches and the NBO analysis on conformers **1a–1d**
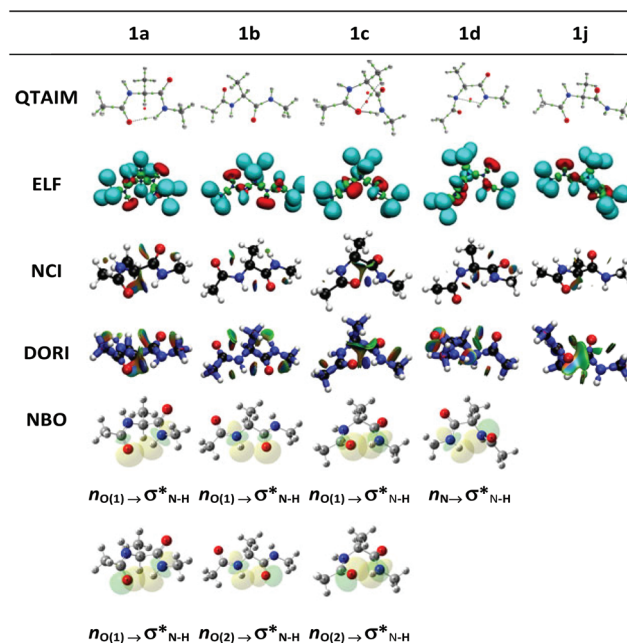
and **1j** (Fig. 3; more details in Table S7 and Fig. S3–S6 in the ESI†). The key parameters obtained by each method are shown in Table 4. NCI and DORI, which use the electron density value on the BCP to discriminate bond strength, indicate that conformer **1c** forms the strongest IHB. QTAIM is being criticised in the literature about its performance in characterising weak or long range interactions.[25] Accordingly, it could not find an IHB for conformer **1b**, while all the other applied

Table 4 IHB parameters for compounds **1** and **2** from QTAIM (ρ), ELF (CVBI), NCI and DORI [sign(λ_2)ρ] in au and NBO orbital interactions corresponding to IHBs (n → σ*) in kcal mol^{-1}. Calculated IHB distances are also shown, in Å

	Compound 1					Compound 2	
	1a	**1b**	**1c**	**1d**	**1j**[a]	**2a**	**2b**
ρ	0.022	—	0.029	0.017	—	0.012	0.021
CVBI[b]	+0.044	+0.087	+0.034	+0.075	+0.140	+0.105	+0.065
Sign(λ_2)ρ[b]	−0.022	−0.019	−0.029	−0.017	−0.06	−0.012	−0.021
$n_{O(1)} \to \sigma^*_{NH}$	2.52	0.59	4.30	—	—	0.95	0.82
$n_{O(2)} \to \sigma^*_{NH}$	3.92	2.04	6.50	—	—	1.71	2.37
$n_N \to \sigma^*_{NH}$	—	—	—	1.31	—	—	—
IHB distance	2.05	2.22	1.91	2.31	—	2.17	2.38

[a] Values correspond to the C=O···C interaction in conformer **1j**. [b] Smaller/more negative values correspond to stronger IHBs.

This journal is © The Royal Society of Chemistry 2015

Org. Biomol. Chem., 2015, **13**, 9206–9213 | **9209**

Table 5 Total relative energies [ΔE(Tot)],[a] free energy of the hypothetical case where hyperconjugation is removed [ΔE(L)],[a] and hyperconjugative energy [ΔE(NL)],[a] (in kcal mol^{-1}) for compounds **1** and **2** in the gas phase (isolated) and in different media (IEF-PCM), B3LYP-D3/aug-cc-pVDZ level

		Isolated	CH_2Cl_2	Acetone	CH_3CN	DMSO	CH_3OH	H_2O
1a	ΔE(Tot)	0.00	0.00	0.00	0.00	0.00	0.00	0.00
	ΔE(L)	11.21	11.96	11.59	11.42	11.37	11.44	11.30
	ΔE(NL)	14.53	12.94	12.07	11.70	11.59	11.75	11.43
1b	ΔE(Tot)	1.61	0.77	0.69	0.66	0.65	0.66	0.64
	ΔE(L)	1.61	3.24	2.98	2.87	2.84	2.89	2.80
	ΔE(NL)	3.33	3.46	2.77	2.49	2.40	2.53	2.29
1c	ΔE(Tot)	1.99	1.52	1.50	1.49	1.49	1.49	1.49
	ΔE(L)	21.41	23.79	23.58	23.47	23.45	23.49	23.40
	ΔE(NL)	22.75	23.25	22.56	22.26	22.17	22.31	22.05
1d	ΔE(Tot)	3.33	0.99	0.48	0.28	0.22	0.31	0.13
	ΔE(L)	0.00	0.00	0.00	0.00	0.00	0.00	0.00
	ΔE(NL)	0.00	0.00	0.00	0.00	0.00	0.00	0.00
1j	ΔE(Tot)	—	1.60	1.34	1.23	1.19	1.24	1.13
	ΔE(L)	—	2.81	2.71	2.68	2.73	2.69	2.72
	ΔE(NL)	—	2.19	1.85	1.74	1.76	1.76	1.72
2a	ΔE(Tot)	1.06	1.50	1.42	1.07	1.04	1.08	1.01
	ΔE(L)	5.50	2.95	3.97	5.73	5.61	5.73	5.50
	ΔE(NL)	6.50	4.44	5.83	6.80	6.66	6.81	6.50
2b	ΔE(Tot)	0.00	0.00	0.00	0.00	0.00	0.00	0.00
	ΔE(L)	0.00	0.00	0.00	0.00	0.00	0.00	0.00
	ΔE(NL)	0.00	0.00	0.00	0.00	0.00	0.00	0.00

[a] Gibbs free energies for each case were obtained by adding thermodynamic corrections derived from frequency calculations.

theoretical methods found it. ELF, through the core–valence bond index (CVBI),[26] and NBO, through n → σ$^*_{NH}$ interaction energies, are in agreement with NCI and DORI and indicate that conformer **1c** forms the strongest IHB (Table 4).

Conformer **1a**, **1b** and **1d** form weaker IHBs than conformer **1c**, with the general trend **1c** > **1a** > **1b** > **1d**. Such trend is predicted by ELF, NCI, DORI, NBO and also the distance criteria of IHB strength (Table 4). Interestingly, conformer **1c**, which forms the strongest IHB, contributes only with 1.5% to the total conformational population for the isolated compound and is even lower in the other calculated media (Table 3). Conformer **1a**, which forms the second strongest IHB, which is a seven-membered ring IHB, is the most stable for the isolated compound. Since conformer **1a** has a comparable dipole moment value with **1b**, such IHB could influence in the relative stability of conformer **1a** for the isolated compound. We now turn to other effects such as steric and hyperconjugative interactions, which could also play important roles in determining the conformer populations.

NBO analysis may be used to evaluate the contribution of steric and hyperconjugative interactions for the stability of a given geometry. One can decompose the relative total Gibbs free energy [ΔE(Tot)] of one conformer into its Natural Lewis structure Gibbs free energy [ΔE(L)], which is correlated to the classical steric/electrostatic energies of the conformer, and its Natural non-Lewis Gibbs free energy [ΔE(NL)], which is correlated to its hyperconjugative stabilisation. ΔE(Tot), ΔE(L) and

ΔE(NL) values in different media (IEF-PCM) are shown for the conformers of compound **1** in Table 5. This NBO analysis indicates that for the isolated compound, the high relative energy of conformer **1c** in comparison to conformers **1a** and **1b** is due to steric/electrostatic interactions in **1c** that are more destabilising than in the other conformers [Table 5; ΔE(L) values]. In contrast, conformer **1c** is highly stabilised by hyperconjugative interactions [Table 5; ΔE(NL) values], the main source of which comes from its N–H⋯O=C IHB (Table 4; $n_{O(1)} \rightarrow \sigma^*_{NH}$ and $n_{O(1)} \rightarrow \sigma^*_{NH}$ interaction energy values). Thus, although conformer **1c** forms the strongest IHB, it is not the most stable conformer due to steric hindrance in this conformer. Such high relative steric hindrance of conformer **1c** may be explained by comparing the 7-membered ring formation from the N–H⋯O=C IHB in conformers **1a** and **1c**. If we compare the 7-membered rings in conformer **1a**, the global minimum for the isolated compound, and in conformer **1c**, one may observe that the alanine CH$_3$ side chain group is in a pseudo-axial position in **1c**, while it is in a pseudo-equatorial position in **1a** (Fig. 1).

NBO analysis indicates that the higher relative stability for isolated conformer **1a** comes from its higher relative hyperconjugative stabilisation [ΔE(NL) values; Table 5], which decreases in higher polar media (not due to any particular orbital–orbital interaction, but the sum of all of them). Indeed, conformer **1a** suffers ~10 kcal mol^{-1} higher steric hindrance than the other stable conformers in solution (**1b**, **1d** and **1j**).

Thus, hyperconjugation, together with the N–H···O IHB, are the main responsible interactions that account for the relative stability of **1a**. As shown in Table 4 and Fig. 3, conformers **1b** and **1d** form the weakest IHBs and **1j** does not form an IHB at all (ELF, NCI and DORI indicate that **1j** may form a weak intramolecular C=O···C stabilising interaction, which may be found in protein and protein ligands[27]). The relative energies of these conformers in comparison to conformer **1a** then comes from three main factors: (1) low relative steric/electrostatic interactions as showed by their small ΔE(L) values in comparison to **1a** (Table 5); (2) higher dipole moments in comparison to **1a**, which make **1b**, **1d** and **1j** more stable in more polar solvents; (3) smaller entropic penalty from Gibbs free energies than conformer **1a**, since **1a** has a more ordered "folded" geometry as a consequence of its strong N–H···O 7-membered IHB. Moreover, it is expected that by considering explicit solvation, the population of conformer **1a** should decrease in polar protic media such as methanol and water, due to destabilisation of its IHB, with consequent increased population of conformers **1b** and **1d** and **1j**.

In order to simulate the lack of IHB formation of conformer **1a**, and also in conformers **1c** and **1d**, we replaced the H(N) involved in IHB in these conformers by a CH$_3$ group. Conformers **2a** (~25%) and **2b** (~75%) are the only ones that contribute significantly to the population in any medium (Fig. 2 and Table 3). Conformer **2a** and **2b** are parents of conformers **1a** and **1b**, respectively. However, conformer **2a** is possibly forming a weak 8-membered C–H···O=C IHB rather than a strong 7-membered N–H···O=C, while conformer **2b** does not differ considerably from its analogue **1b**. Interestingly, conformer **2b** is now the more stable conformer, rather than **2a**. Such stability inversion may confirm that IHB formation in conformer **1a** is crucial to stabilise it in comparison to conformer **1b**.

Thus, the strong N–H···O=C IHB in the 7-membered ring of conformer **1a** is disrupted by replacing the H atom by a CH$_3$ group, causing its relative population to decrease accordingly. A similar disruption of the N–H···O=C IHB of **1a** is caused by intermolecular hydrogen bond formation of **1a** with polar aprotic or polar protic solvents and, hence, this simple analysis may simulate the solvent effect on conformational preferences and geometry of Ac-Ala-NHMe. However, some main geometric parameters are different between conformers **1a** and **2a**, e.g. their ψ[N–C–C(O)–N] dihedral angle (74.0° and 114.3° for **1a** and **2a**, respectively) and ϕ[C(O)–N–C–C(O)] dihedral angle (82.4° and 94.6° for **1a** and **2a**, respectively), which could indicate that such compounds are not comparable. On the other hand, it is expected that such parameters will change by changing the solvent polarity and solute–solvent interactions as well. A more quantitative analysis of the "solvent-induced" IHB disruption would require complex and time-consuming molecular dynamic simulations including explicit solvent molecules.

QTAIM, NCI, ELF, DORI and NBO methods were also applied to conformers **2a** and **2b** (Fig. 4; Table S8 and Fig. S7–S10 in the ESI†). All methods indicate formation of weak non-usual IHB with a CH···O=C motif for **2a** and a more common
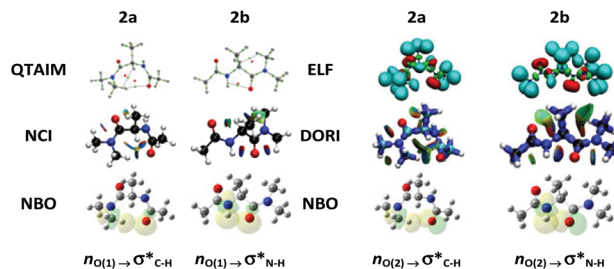

Fig. 4 QTAIM, ELF, NCI, DORI and NBO graphical representations for conformers **2a** and **2b**. QTAIM green points and red points represent bond critical points and cage critical points, respectively. NCI figures were obtained with a blue−green−red scale ranging from −0.02 < sign λ_2 < 0.02 au and with a RDG cutoff of 0.5 au. ELF localization domains were built with a 0.8 au isodensity value. DORI were also obtained with a blue−green−red scale ranging from −0.02 < sign λ_2 < 0.02 au. NBO plots of orbitals in n → σ^*_{NH} interactions were obtained with an isovalue of 0.04 au. All figures obtained from B3LYP/aug-cc-pVDZ electron densities at B3LYP-D3/aug-cc-pVDZ optimised geometries.

NH···O=C IHB for **2b**. Such non-usual IHB for conformer **2a** would not be expected to survive in a polar solvent, which could be a source of differentiation in the energy and geometry of conformer **1a** in polar solvents and compound **2a**. Indeed, The CH···O=C IHB in **2a** is predicted to be rather weak by the different methods applied (Table 4) and should have negligible influence on **2a** geometry and energy.

Thus, conformer **2a** is not the more stable conformer in any medium. Instead, conformer **2b**, which has an "extended" geometry and forms a weak NH···O=C IHB is the more stable one. The outcome for conformer **2b** may help to understand the conformational preference of compound **1** in polar solvents, where intramolecular hydrogen bond is unfavorable due to intermolecular hydrogen bond formation with the solvent. In this way, Ac-Ala-NHMe would prefer conformer **1a** for the isolated compound or in apolar solvents such as CH$_2$Cl$_2$, but in polar protic solvents such as water the extended conformation of conformer **1b** should be the preferential one.

Conclusions

In summary, we have used established DFT methods to study the conformational behaviour of a prototypical building block for the alanine residue in peptides, Ac-Ala-NHMe (**1**), and its doubly N-methylated derivative, Ac-Ala-NMe$_2$ (**2**), in the gas phase and in polarisable continua modelling for a variety of solvents. Of the many possible conformers identified in Monte Carlo searches, only five and two were found to contribute significantly to equilibrium mixtures of **1** and **2**, respectively, at ambient conditions. While the composition of this equilibrium shows some solvent dependence for **1**, it is rather insensitive to the nature of the surrounding medium for **2**. Using a set of advanced interpretation tools based on the analysis of wave functions and electron densities, the relative stabilities of

This journal is © The Royal Society of Chemistry 2015

Org. Biomol. Chem., 2015, **13**, 9206–9213 | **9211**

the different conformers are indicated to arise from a complex interplay between the strengths of possible intramolecular hydrogen bonds, steric interactions, hyperconjugation, and, in polar environments, the overall dipole moments.

In order to probe how differences in equilibrium composition may be reflected in spectroscopic observables, we have calculated and measured the key NMR parameters in the solvents of interest. The ^3J(H,H) spin–spin coupling constant involving the alanine NH and C_αH atoms should be of particular diagnostic value for the adopted backbone conformation. Due to the insensitivity of the conformational equilibrium of **2** on the surrounding medium, little variation is predicted for this property. Despite the somewhat larger dependence of the equilibrium composition of **1** on the surrounding dielectric, only minor changes in the computed (averaged) ^3J values are computed. These findings are corroborated by the observed ^3J couplings, which indeed show little sensitivity toward the solvent. Theory and experiment are thus in concert, and the latter is much enhanced by the former through insights from DFT-based modelling of structures and energies, as well as analysis of wave functions and electron densities. At least, other experimental techniques, such as infrared and vibrational circular dichroism spectroscopies, may support the present results, obtained by experimental ^{1}H NMR spectroscopy, in disentangling the conformational preferences in solution of these important peptide models.

Acknowledgements

Notes and references

1 (a) A. Lesarri, R. Sanchez, E. J. Cocinero, J. C. Lopez and J. L. Alonso, *J. Am. Chem. Soc.*, 2005, **127**, 12952; (b) B. Boeckx and G. Maes, *J. Phys. Chem. B*, 2012, **116**, 12441; (c) G. Bazsó, G. Magyarfalvi and G. Tarczay, *J. Phys. Chem. A*, 2012, **116**, 10539; (d) V. Barone, M. Biczysko, J. Bloinoac and C. Puzzarini, *Phys. Chem. Chem. Phys.*, 2013, **15**, 1358; (e) E. E. Najbauer, G. Bazsó, S. Góbi, G. Magyarfalvi and G. Tarczay, *J. Phys. Chem. B*, 2014, **118**, 2093 and references therein.

2 (a) H. Farrokhpour, F. Fathi and A. N. De Brito, *J. Phys. Chem. A*, 2012, **116**, 7004; (b) C. M. Nunes, L. Lapinski, R. Fausto and I. Reva, *J. Chem. Phys.*, 2013, **138**, 125101; (c) G. Bazsó, E. E. Najbauer, G. Magyarfalvi and G. Tarczay, *J. Phys. Chem. A*, 2013, **117**, 1952; (d) W. Y. Sohn, S. Ishiuchi, P. Çarçabal, H. Oba and M. Fujii, *Chem. Phys.*, 2014, **445**, 21 and references therein.

3 (a) V. L. Cruz, J. Ramos and J. Martinez-Salazar, *J. Phys. Chem. B*, 2012, **116**, 469; (b) A. T. Tzanov, M. A. Cuendet and M. E. Tuckerman, *J. Phys. Chem. B*, 2014, **118**, 6539; (c) J. Groule and F. Jensen, *J. Chem. Theory Comput.*, 2011, **7**, 1783.

4 (a) V. Parchaňský, J. Kapitán, J. Kaminský, J. Šebestík and P. Bouř, *J. Phys. Chem. Lett.*, 2013, **4**, 2763; (b) M.-P. Geigeot, *J. Phys. Chem. Lett.*, 2009, **113**, 10059; (c) H. Fujitani, A. Matsuura, S. Sakai, H. Sato and Y. Tanida, *J. Chem. Theory Comput.*, 2009, **5**, 1155; (d) F. Ioannou, G. Archontis and E. Leontidis, *J. Phys. Chem. B*, 2011, **115**, 13389; (e) H. Okumura, *Phys. Chem. Chem. Phys.*, 2011, **13**, 114.

5 (a) R. A. Cormanich, L. C. Ducati and R. Rittner, *Chem. Phys.*, 2011, **387**, 85; (b) R. A. Cormanich, L. C. Ducati and R. Rittner, *J. Mol. Struct.*, 2012, **1014**, 12; (c) R. A. Cormanich, L. C. Ducati, C. F. Tormena and R. Rittner, *Chem. Phys.*, 2013, **421**, 32.

6 (a) R. A. Cormanich, L. C. Ducati, C. F. Tormena and R. Rittner, *J. Phys. Org. Chem.*, 2013, **26**, 849; (b) C. J. Duarte, R. A. Cormanich, L. C. Ducati, C. F. Tormena and R. Rittner, *J. Mol. Struct.*, 2013, **1050**, 174; (c) R. A. Cormanich, L. C. Ducati, C. F. Tormena and R. Rittner, *Spectrochim. Acta*, 2014, **123**, 482.

7 R. A. Cormanich, R. Rittner and M. Bühl, *RSC Adv.*, 2015, **5**, 13052.

8 (a) V. Pophristic and L. Goodman, *Nature*, 2001, **411**, 565; (b) R. A. Cormanich and M. P. Freitas, *J. Org. Chem.*, 2009, **74**, 8384; (c) M. P. Freitas, M. Buhl, D. O'Hagan, R. A. Cormanich and C. F. Tormena, *J. Phys. Chem. A*, 2012, **116**, 1677.

9 J. K. M. Sanders and J. D. Mersh, *Prog. Nucl. Magn. Reson. Spectrosc.*, 1982, **15**, 353.

10 Y. Shao, L. F. Molnar, Y. Jung, J. Kussmann, C. Ochsenfeld, S. T. Brown, A. T. B. Gilbert, L. V. Slipchenko, S. V. Levchenko, D. P. O'Neill, R. A. DiStasio Jr., R. C. Lochan, T. Wang, G. J. O. Beran, N. A. Besley, J. M. Herbert, C. Y. Lin, T. Van Voorhis, S. H. Chien, A. Sodt, R. P. Steele, V. A. Rassolov, P. E. Maslen, P. P. Korambath, R. D. Adamson, B. Austin, J. Baker, E. F. C. Byrd, H. Dachsel, R. J. Doerksen, A. Dreuw, B. D. Dunietz, A. D. Dutoi, T. R. Furlani, S. R. Gwaltney, A. Heyden, S. Hirata, C.-P. Hsu, G. Kedziora, R. Z. Khalliulin, P. Klunzinger, A. M. Lee, M. S. Lee, W. Z. Liang, I. Lotan, N. Nair, B. Peters, E. I. Proynov, P. A. Pieniazek, Y. M. Rhee, J. Ritchie, E. Rosta, C. D. Sherrill, A. C. Simmonett, J. E. Subotnik, H. L. Woodcock III, W. Zhang, A. T. Bell, A. K. Chakraborty, D. M. Chipman, F. J. Keil, A. Warshel, W. J. Hehre, H. F. Schaefer, J. Kong, A. I. Krylov, P. M. W. Gill and M. Head-Gordon, *Phys. Chem. Chem. Phys.*, 2006, **8**, 3172.

11 M. J. Frisch, G. W. Trucks, H. B. Schlegel, G. E. Scuseria, M. A. Robb, J. R. Cheeseman, G. Scalmani, V. Barone, B. Mennucci, G. A. Petersson, H. Nakatsuji, M. Caricato, X. Li, H. P. Hratchian, A. F. Izmaylov, J. Bloino, G. Zheng, J. L. Sonnenberg, M. Hada, M. Ehara, K. Toyota, R. Fukuda,

9212 | *Org. Biomol. Chem.*, 2015, **13**, 9206–9213

This journal is © The Royal Society of Chemistry 2015

J. Hasegawa, M. Ishida, T. Nakajima, Y. Honda, O. Kitao, H. Nakai, T. Vreven, J. A. Montgomery Jr., J. E. Peralta, F. Ogliaro, M. Bearpark, J. J. Heyd, E. Brothers, K. N. Kudin, V. N. Staroverov, R. Kobayashi, J. Normand, K. Raghavachari, A. Rendell, J. C. Burant, S. S. Iyengar, J. Tomasi, M. Cossi, N. Rega, J. M. Millam, M. Klene, J. E. Knox, J. B. Cross, V. Bakken, C. Adamo, J. Jaramillo, R. Gomperts, R. E. Stratmann, O. Yazyev, A. J. Austin, R. Cammi, C. Pomelli, J. W. Ochterski, R. L. Martin, K. Morokuma, V. G. Zakrzewski, G. A. Voth, P. Salvador, J. J. Dannenberg, S. Dapprich, A. D. Daniels, Ö. Farkas, J. B. Foresman, J. V. Ortiz, J. Cioslowski and D. J. Fox, *Gaussian 09, Revision D.01*, Gaussian, Inc., Wallingford CT, 2009.

12 G. Scalmani and M. J. Frisch, *J. Chem. Phys.*, 2010, **132**, 114110.

13 A. D. Becke, *J. Chem. Phys.*, 1993, **98**, 1372.

14 V. Barone, in *Recent Advances in Density Functional Methods, Part I*, ed. D. P. Chong, World Scientific Publ. Co., Singapore, 1996.

15 R. Suardíaz, C. Pérez, R. Crespo-Otero, J. M. García de la Vega and J. San Fabián, *J. Chem. Theor. Comput.*, 2008, **4**, 448.

16 F. Nozirov, T. Kupka and M. J. Stachów, *Chem. Phys.*, 2014, **140**, 144303.

17 A. E. Reed, L. A. Curtiss and F. Weinhold, *Chem. Rev.*, 1988, **88**, 889.

18 R. F. W. Bader, *Atoms in Molecules: A Quantum Theory*, Clarendon, Oxford, 1990.

19 B. Silvi and A. Savin, *Nature*, 1994, **371**, 683.

20 E. Johnson, S. Keinan, P. Mori-Sánchez, J. Contreras-García, A. Cohen and W. Yang, *J. Am. Chem. Soc.*, 2010, **132**, 6498.

21 P. de Silva and C. Corminboeuf, *J. Chem. Theory Comput.*, 2014, **10**, 3745.

22 T. A. Keith, *AIMAll (Version 14.11.23)*, TK Gristmill Software, Overland Park KS, USA, 2013 (aim.tkgristmill.com).

23 S. Noury, X. Krokidis, F. Fuster and B. Silvi, *ToPMoD*, Laboratoire de Chemie Théorique, Université Pierre et Marie Curie, París, http://www.lct.jussieu.fr/pagesperso/silvi/topmod_english.html, 1999.

24 M. Karplus, *J. Chem. Phys.*, 1959, **30**, 11.

25 (*a*) J. R. Lane, J. Contreras-Garcia, J.-P. Piquemal, B. J. Miller and H. G. Kjaergaard, *J. Chem. Theory Comput.*, 2013, **9**, 3263; (*b*) F. Weinhold, P. R. Schleyer and W. C. McKee, *J. Comput. Chem.*, 2014, **35**, 1499.

26 F. Fuster and B. Silvi, *Theor. Chem. Acc.*, 2000, **104**, 13.

27 F. R. Fischer, P. A. Wood, F. H. Allen and F. Diederich, *Proc. Natl. Acad. Sci. U. S. A.*, 2008, **105**, 17290.

This journal is © The Royal Society of Chemistry 2015

Org. Biomol. Chem., 2015, **13**, 9206–9213 | **9213**